



City Research Online

## City, University of London Institutional Repository

---

**Citation:** Liu, F., Feng, R. & Tsavdaridis, K. D. (2021). Form finding of assembled lattice structure considering the effect of joint stiffness. *Structures*, 31, pp. 1096-1105. doi: 10.1016/j.istruc.2021.02.026

This is the accepted version of the paper.

This version of the publication may differ from the final published version.

---

**Permanent repository link:** <https://openaccess.city.ac.uk/id/eprint/27949/>

**Link to published version:** <https://doi.org/10.1016/j.istruc.2021.02.026>

**Copyright:** City Research Online aims to make research outputs of City, University of London available to a wider audience. Copyright and Moral Rights remain with the author(s) and/or copyright holders. URLs from City Research Online may be freely distributed and linked to.

**Reuse:** Copies of full items can be used for personal research or study, educational, or not-for-profit purposes without prior permission or charge. Provided that the authors, title and full bibliographic details are credited, a hyperlink and/or URL is given for the original metadata page and the content is not changed in any way.

---

---

---

City Research Online:

<http://openaccess.city.ac.uk/>

[publications@city.ac.uk](mailto:publications@city.ac.uk)

---

# Form finding of assembled lattice structure considering the effect of joint stiffness

Fengcheng Liu<sup>1,2</sup>, Ruoqiang Feng<sup>1\*</sup>, Konstantinos Daniel Tsavdaridis<sup>2</sup>

<sup>1</sup>The Key Laboratory of Concrete and Prestressed Concrete Structures of Ministry of Education, Southeast University, Nanjing, 211189, China

<sup>2</sup>School of Civil Engineering, Faculty of Engineering and Physical Sciences, University of Leeds, Woodhouse Lane, LS2 9JT, Leeds, UK

**Abstract:** The joint stiffness can have a significant effect on the stability of single-layer lattice structure. However, it is yet unclear what is the degree of influence of joint stiffness on the form finding of assembled lattice structures. This paper presents a form finding method that suits assembled free-form single-layer lattice structures while the effect of joint stiffness on the form finding of the structure is investigated. Based on experimental results of the Ring-Sleeve joint, spring elements are initially used to simulate the joint stiffness and then finite element models of the assembled single-layer lattice structures with semi-rigid joints are established. The effect of joint stiffness on the structural form finding is studied by changing the spring stiffness. Thereafter, the optimal shapes of the assembled lattice structures with different joint stiffness and improved buckling load capacity are obtained. Finally, the mechanical properties of the resulted structures with different joint stiffness are extensively compared. The results show that different joint stiffness generate different structural shapes, and the greater joint stiffness results in higher structural height. Furthermore, both the structural buckling load capacity and the imperfection sensitivity increase with the increase of joint stiffness. Overall, the buckling load capacity of the semi-rigid model is lower than that of the replaced model that obtained based on the rigid structure.

**Keywords:** Assembled lattice structures; Semi-rigid joints; Beam-Virtual spring element; Form finding

## 1. Introduction

In recent years, the rise of computer-aided design and modelling techniques have enabled a new level of sophistication in the design of free-form lattice structures [1]. And thanks to their splendid visual effects and the capacity to cover large spaces with uninterrupted span, lots of free-form lattice structures are widely used in civil infrastructure including large-scale commercial buildings and stadia, such as the Pearl stadium and the Usnisa palace shown in Fig. 1.

Basically, most of geometrical and topological information of lattice structures is stored in their joints, and the joint stiffness is sure to have an important effect on the structural mechanical performance. Moreover, the 21<sup>st</sup> century is the era of efficiency in design. Therefore, the assembled free-form lattice structures has become a very popular structural typology widely chosen in many recent applications. As the name implies, an assembled structure is the one that the connections of its rods are not connected through the welding joints but the assembled ones. So far, according to the previous researches, there are already many kinds of joints which can be applied for the free-form lattice structures, such as the German's metro-system, as shown in Fig. 2(a), and the SBP-system as shown in Fig. 2(b) [2-3]. More recently, the newly developed design algorithms, such as the structural topology optimisation algorithm, have effectively responded to the demand for the design of complex joints. Abdelwahab and Tsavdaridis [4] developed some novel node-connections with the help of structural optimisation algorithm, as shown in Fig. 2(c). Seifi [5] used the Bi-directional Evolutionary Structural Optimisation (BESO) techniques to design the structural joints of complex shapes for lattice-shell structures, as shown in Fig. 2(d).



(a) Pearl Stadium, China

(b) Nanjing's Usnisa Palace, China

Fig. 1 Examples of free-form lattice structures



(a) Metro-2 connector (b) SBP-3 connector (c) The novel node-connections (d) Result of BESO method  
 Fig. 2 some examples of assembled joints

On account of the fact that so many types of joints have been developed and widely used in the practical projects, the assembled single-layer free-form lattice structures have become an interesting topic of research for large-span space structures. Furthermore, judging from research results in the past, most of the joints in assembled lattice structures are semi-rigid joints. Actually, the joints can be considered as one of the most important elements in the assembled lattice structures due to their vital role in load transferring process. There is a great amount of forces transferred through the small volume. Therefore, it is no doubt that the mechanical properties of the joints in assembled structures, such as strength and bending stiffness have a great influence on the mechanical behaviour of the structure. Observations from earlier studies [6-7] confirmed that the joint stiffness has a considerable effect on the load-displacement behaviour of the structure. Then, various types of joints have experimented for their respective mechanical performances, which have shown different effects on reticulated shells. According to a prototype test, the bending stiffness of the joint was determined [8], and the joint bending stiffness was brought into the overall structural analysis model. The differences of stable bearing capacity between the perfect lattice shell and the lattice shell with geometric initial imperfections were compared. The authors concluded that the rigid shell of the reticulated shell was very sensitive to the initial geometric imperfections, and as the stiffness of the joint weakens, the sensitivity of the reticulated shell to such imperfections decreases until the joint is hinged, thus this effect can be ignored. L'opez et al. [9-10], Kato et al. [11] and Lightfoot et al. [12] verified that the stiffness of the joints is an important factor that influences the behaviour of a single-layer latticed dome, and the influence of semi-rigid connection on structural stability is greater than that of geometric imperfect on structural stability. Furthermore, there are many other scholars who have meticulously studied the mechanical properties of semi-rigid joints. Guo et al. [13-14] studied the aluminum alloy plate joint systematically. The bending properties and key factors affecting the bending capacity of aluminum alloy plate joints were analysed in-depth, and the calculation formula of bearing capacity is put forward. In addition, various types of joints have experimented for their respective mechanical performances according to Ma and Feng [15-17], which have shown different effects on reticulated shells.

As for the form finding of free-form single-layer lattice structures, many techniques have been developed so far, namely the dynamic relaxation method, the force density method, the updated reference strategy, and the particle-spring system method. In addition, Feng et al. [18-19] studied the form finding of cable-braced free-form lattice structures with the aim of structural strain energy. Hawdon-Earl and Tsavdaridis [20] developed a standard and robust methodology for shell optimisation design. The methodology uses Oasys GSA and Abaqus which allow both form-finding analysis and dimensioning to be conducted. However, these methods are generally proposed for lattice structures with rigid joints to find the equilibrium states; few practical approaches for the shape designs of assembled free-form lattice structures with semi-rigid joints have been developed.

Therefore, it is worth noting that earlier studies on assembled free-form lattice structures have mainly concentrated on the assembled connections and their influence on the structures' stability, yet no studies have been reported on the form finding of assembled single-layer lattice structures considering the effects of joint stiffness. Consequently, this paper takes the effect of the joint stiffness into consideration to optimise the assembled single-layer lattice structure, and account for the effect of different joint stiffness on the structural form finding.

## 2. Get the actual joint stiffness

In order to know the actual joint stiffness, a prototype test of the joint was conducted by the author's group. The joint used in the test is called Ring-Sleeve joint, which is a self-developed joint that is suitable for the

assembled free-form single-layer lattice structure. The mechanical properties of the joint have been thoroughly studied through both experiments and finite element analysis by Wang et al. [21].

## 2.1 Parameters of Ring-sleeve joint

The details of the construction of Ring-sleeve joint are shown in a sectional drawing in Fig. 3. The joint consists of a central ring, sleeves, tubes and high-strength bolts. There are identical bolt holes in the central ring, sleeve, and tube. The bolt holes of the central ring, sleeves, and tubes are aligned to assemble the joint using the high-strength bolts.

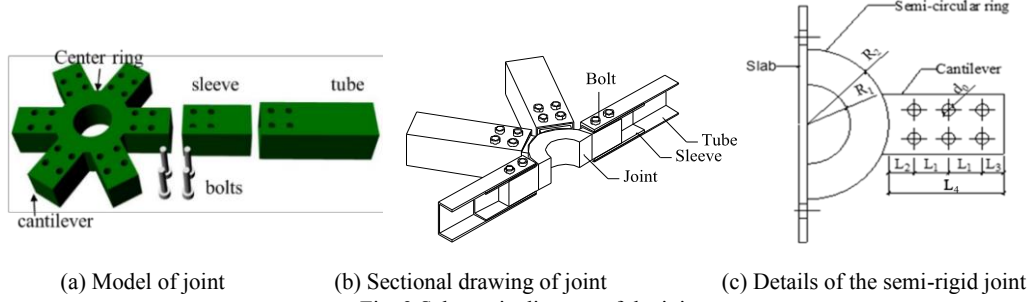


Fig. 3 Schematic diagram of the joint

## 2.2 Stiffness of the Ring-sleeve joints

Table 1. Geometrical parameters of the joint

| Tube section | Joint No. | Joint |       |       | Bolt     |          |       | Tube length | Sleeve |           |
|--------------|-----------|-------|-------|-------|----------|----------|-------|-------------|--------|-----------|
|              |           | $R_1$ | $R_2$ | $L_4$ | Quantity | Diameter | Space | $L$         | $L_5$  | Thickness |
| 100×100×4    | Test A    | 50    | 95    | 135   | 4        | 16       | 80    | 715         | 180    | 4         |
|              | Test B    | 50    | 95    | 105   | 4        | 16       | 50    | 715         | 180    | 4         |
|              | Test C    | 50    | 95    | 105   | 4        | 16       | 50    | 715         | 140    | 4         |
|              | Test D    | 50    | 95    | 105   | 4        | 16       | 50    | 715         | 100    | 4         |

In order to determine several mechanical indexes of the bolted joint, four prototype tests were carried out and the design parameters of the test joints are shown in Table 1 and Fig. 3(c).

Based on the rotational stiffness of rigid joints, the joint stiffness factor  $F_c$  is defined as the ratio of the assembled joint stiffness to rigid joint stiffness, as shown in formula (1).

$$F_c = \frac{\text{assembled joint stiffness}}{\text{rigid joint stiffness}} \quad (1)$$

For the rigid joint, the out-plane elastic bending stiffness can be defined as:

$$K_{out} = \frac{3EI_{out}}{L} \quad (2)$$

The in-plane elastic bending stiffness can be defined as:

$$K_{in} = \frac{3EI_{in}}{L} \quad (3)$$

The torsional stiffness can be defined as:

$$K_{tor} = \frac{GI_{tor}}{L} \quad (4)$$

Where  $E$  is the elastic modulus of a tube, and  $G$  is the shear modulus of elasticity.  $I_{out}$  is the out-plane inertia moment of a tube.  $I_{in}$  is the in-plane inertia moment of a tube.  $I_{tor}$  is the torsional inertia moment of a tube.  $L$  is the length of a tube.

### 3. Establishment of assembled lattice structures with different joint stiffness

#### 3.1 the Beam-Virtual spring elements

In this section, the way to simulate the different rotational stiffness of the assembled joint in the finite element model is presented. In order to study the influence of the assembled joint stiffness on form finding of assembled single-layer lattice structures, in this paper, the Beam-Virtual Spring elements were used to simulate the joint stiffness according to Wang et al. [21]. Actually, there are six virtual spring elements were used to simulate the freedom of six directions of the joints. In specific, in the numerical model of assembled free-form single-layer lattice structures, three nonlinear spring elements ‘combin39’ with unidirectional freedom were used to simulate the rotational capacity of the assembled semi-rigid joint in three directions, and the other three axial spring elements were used to simulate the three-direction translational freedom of the joint.

#### 3.2 Obtain the spring stiffness

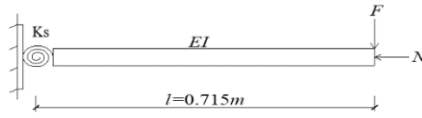


Fig. 4 Computational model with rotating spring

Fig. 4 depicts the nodal calculation model with rotating springs. Under the action of bending moment  $M$ , the deformation  $\theta$  of the right end of rod mainly includes deformation  $\theta_1$  caused by bending of rod and deformation  $\theta_2$  in the joint area. Assuming that the length of the rod is  $l$ , the elastic modulus is  $E$ , the cross-section inertia distance is  $I$ , rotational stiffness of rod is  $K_B$ , the spring at end of the rod is a zero-length element, the rotational stiffness is  $K_S$ , and the rotational stiffness of the whole model is  $K_J$ .

Then, according to structural mechanics:

The rotation angle of the rod itself is:

$$\theta_1 = \frac{M}{K_B} \quad (5)$$

The rotation angle of the spring is:

$$\theta_2 = \frac{M}{K_S} \quad (6)$$

Total rotation of the joint is:

$$\theta = \frac{M}{K_J} = \theta_1 + \theta_2 \quad (7)$$

Then, the spring stiffness can be obtained as:

$$K_S = \frac{K_J \times K_B}{K_B - K_J} \quad (8)$$

The rotational stiffness of the assembled joint model  $K_J$  has been obtained by the prototype test, and the final spring stiffness can be obtained. It is worth noting that there are only four different types of joint stiffness that were obtained by the test. Therefore, in order to analyse the influence of different joint stiffness on form finding of lattice structures more comprehensively, seven other semi-rigid joints were derived in this paper according to the test results, as shown in Table 2, the 4<sup>th</sup> to 7<sup>th</sup> joints are the experimental joints, and the remaining joints are the derivation results of this paper. These joints have different stiffness factors which change regularly from 0.1 to 0.9.

Table 2 Spring rotational stiffness

| Joint No. | Initial out-plane rotational stiffness (kN·m/rad) |                        |                | Initial in-plane rotational stiffness (kN·m/rad) |                        |                |
|-----------|---|------------------------|----------------|--|------------------------|----------------|
|           | Semi-rigid joint                                  | Stiffness factor $F_c$ | Spring element | Semi-rigid joint                                 | Stiffness factor $F_c$ | Spring element |
| 1         | 204.19  | 10%                    | 226.88         | 61.25  | 3%                     | 63.15          |

|    |         |     |          |        |     |        |
|----|---------|-----|----------|--------|-----|--------|
| 2  | 408.39  | 20% | 510.48   | 81.67  | 4%  | 85.08  |
| 3  | 612.58  | 30% | 875.12   | 102.09 | 5%  | 107.47 |
| 4  | 781.00  | 38% | 1122.98  | 126.05 | 6%  | 129.97 |
| 5  | 922.00  | 45% | 1888.15  | 148.81 | 7%  | 174.12 |
| 6  | 1030.00 | 50% | 2079.99  | 166.24 | 8%  | 180.66 |
| 7  | 1120.00 | 55% | 2350.90  | 180.77 | 9%  | 192.59 |
| 8  | 1225.17 | 60% | 3062.93  | 204.19 | 10% | 226.88 |
| 9  | 1429.37 | 70% | 4764.56  | 245.03 | 12% | 278.44 |
| 10 | 1633.56 | 80% | 8167.83  | 285.87 | 14% | 332.41 |
| 11 | 1837.76 | 90% | 18377.62 | 326.71 | 16% | 388.94 |

### 3.3 Verification of finite element model of assembled single-layer grid structure

In order to verify the correctness of using the Beam-Virtual Spring elements to simulate the joint stiffness of assembled single-layer grid structure, the finite element model of single-layer spatial grid structure with Beam-Virtual Spring elements is established, and the results of finite element analysis are compared with the experimental results

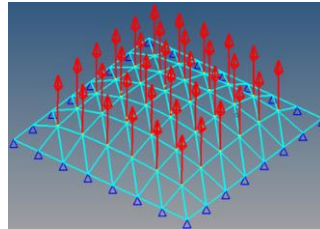


Fig. 5 A free-form single-layer lattice structure

In this section, a free-form single-layer lattice structures shown in Fig. 5 is taken as an example. The initial shape is defined as a free-form surface of 14m in span and 2.7m in height (the rise). The rod is the square steel tube with dimensions of 100mm×100mm×4mm made of Q345 steel, and the elastic modulus is  $2.0 \times 10^5 \text{ MPa}$ . The concentrated load is applied on each node as a uniformly distributed load.

In order to adapt to the laboratory conditions, the original structure was scaled down according to the similarity theory. In this case, 1/4 scaled model was selected. The physical quantities of the scaled model are similar to the original structure. Correspondingly, in the finite element simulation, the joint ending stiffness of the scaled model is taken as 1/256 of the original structure. In the test model, the equivalent node sandbag is used as the loading mode. During loading, the sandbag load is evenly transferred to each node through the loading frame, and the weight of each sandbag is 25kg.

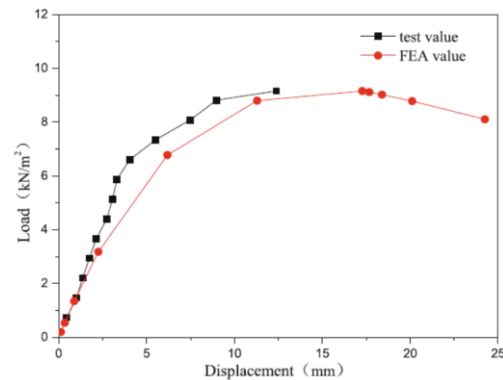


Fig.6 Comparison of load-displacement curves

After the test, the finite element analysis of the scaled model is carried out and compared with the test

results. As shown in Fig. 6, the load displacement curve comparison between the test value and the simulation value is shown. In the test model, the structural initial stiffness is 543.48kN/m; in the finite element model, the structural initial stiffness is 539.44kN/m, the error is only 0.74%, and the structural stiffness in the test model is slightly larger than the simulation value. When the structure loses stability, the ultimate bearing capacity of the two models is consistent, which is 9.15kN/m<sup>2</sup>. For the structural member level, the maximum axial force of the member in the test model is 28.63kN, and that in the finite element simulation is 25.3kN, with a difference of 11.6%. In addition, compared the test model with the finite element model, it is found that the average error of the equivalent stress of each member is 6.74%, which indicates that there is little difference between the results of finite element simulation and the test model.

In summary, through the comparative analysis of the test model and the finite element model, combined with the influence of measurement error in the test, the model test value is basically consistent with the finite element simulation result, which

#### 4. Implementation of form finding

As the FEM (finite element model) of the assembled lattice structure was established, the form finding of the assembled lattice structure considering the effect of different joint stiffness is completed in this section.

##### 4.1 Optimising parameters

In the form finding of free-form single-layer lattice structure, the structural total strain energy can be taken as the objective function, which can be expressed as follows.

**Objective function:**

$$\min C(z) = \frac{1}{2} U^T K U \quad (9)$$

$$\text{Subject to } \begin{cases} \delta \leq \frac{B}{400} \\ \sigma_{\max} \leq 345 \text{MPa} \end{cases} \quad (10)$$

Where  $C$  is the structural total strain energy,  $K$  is the stiffness matrix,  $U$  is the nodal displacement vector,  $z$  is the nodal  $z$ -coordinate.  $B$  is the short span of the structure,  $\delta$  is the maximum nodal displacement and  $\sigma_{\max}$  is the maximum stress of the tubes.

**Design variables:** In this paper, the  $z$ -direction coordinates of the internal nodes of the assembled lattice structure are set as design variables, as shown in Fig. 5. It is worth noting that in an assembled lattice structure, each actual joint was divided into seven points while all of the points have the same coordinates. Therefore, these seven points are considered as the same design variable and have the same shape change in the process of optimisation.

##### 4.2 Implementation of form finding

In this section, a free-form single-layer lattice structures shown in Fig. 5 is taken as an example. The initial shape is defined as a free-form surface of 14m in span and 2.7m in height (the rise). The rod is the square steel tube with dimensions of 100mm×100mm×4mm made of Q345 steel, and the elastic modulus is  $2.0 \times 10^5 \text{MPa}$ . The concentrated load is applied on each node as a uniformly distributed load, including the rod weight, the finishing materials, and the live load of 500 N/m<sup>2</sup>.

The FEA model of the assembled free-form lattice structures was established through the Beam-virtual spring elements, and the virtual springs were used to simulate the joint stiffness. Then, the impact of joint stiffness on form finding of assembled free-form single-layer lattice structures was studied through changing the spring stiffness. Taking the total strain energy as the objective function, and Optistruct solver in Hyper-

Works was used in this paper. Then, through several iterations, the optimal solution is obtained, as shown in Fig. 7.

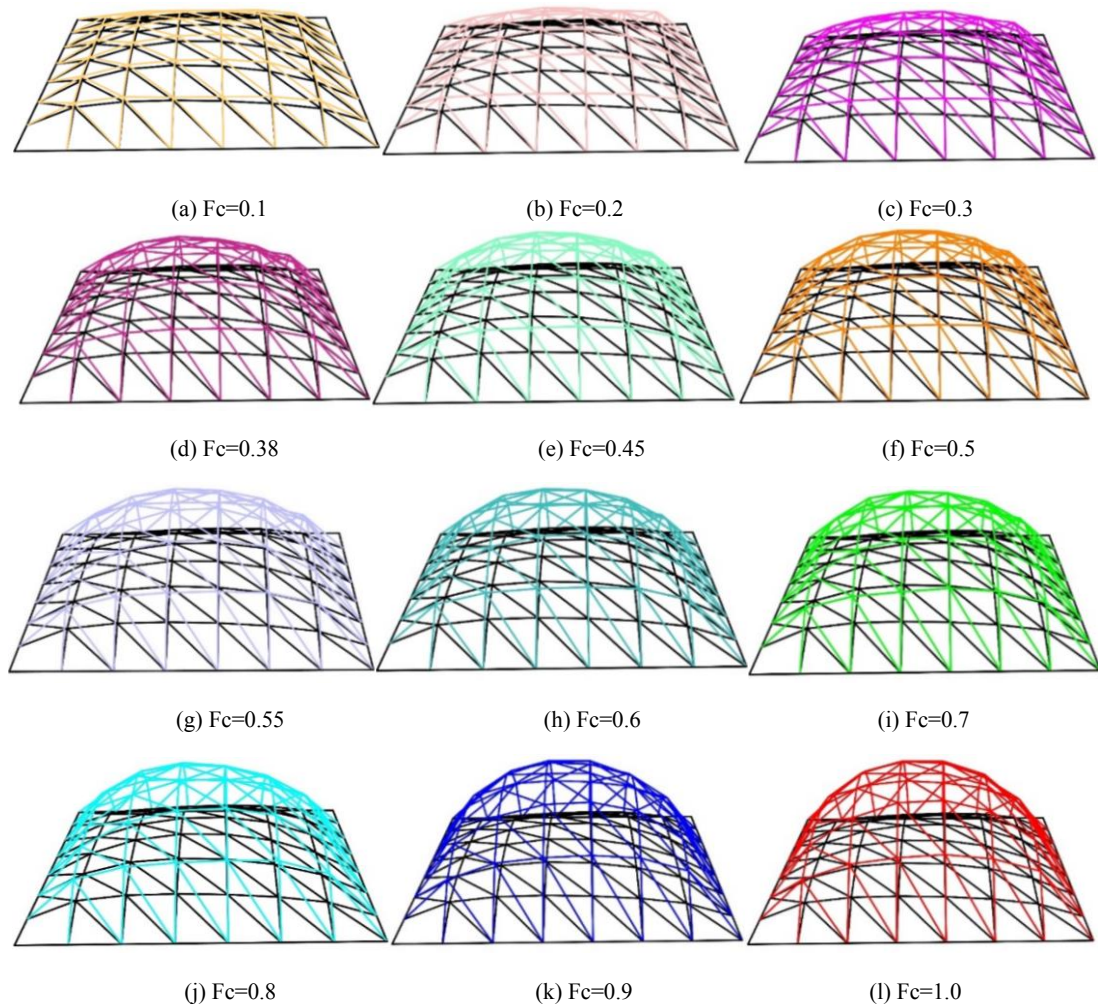


Fig. 7 Comparison of initial shape and the optimised shape under different stiffness factor

Fig. 7 shows a shape comparison of the initial structure and the optimised structures under different stiffness factors. The black line represents the initial state of the structure, and the other colour lattices represent the optimised structural shapes under different stiffness factors. When the stiffness factor is equal to 1.0, it means that it is the result of form finding of lattice structures with rigid joints. Comparing the structural shapes in the figure, it is easily found that with the increase of joint stiffness factor, the variation of structural shape after optimisation is also increasing, and the closer the structural section is to the arch shape. Finally, when the stiffness factor becomes 1.0, the highest structural height was obtained. Therefore, it is proved that joint stiffness has a greater influence on form finding of the lattice structure; the larger joint stiffness can result in significant changes in the shape of a free-form single-layer lattice structures.

Table 3 The initial models

| Model No. | Stiffness factor Fc | Strain energy (KJ) | Buckling load capacity (N/m <sup>2</sup> ) |                   | Imperfection sensitivity | Mass (t) |
|-----------|---------------------|--------------------|--|-------------------|--------------------------|----------|
|           |                     |                    | Without imperfection                       | With imperfection |                          |          |
| 1         | 1.0                 | 80.7               | 103396.22                                  | 73140.15          | 29.30                    | 1.15     |
| 2         | 0.9                 | 81.5               | 99324.12                                   | 70945.8           | 28.57                    | 1.15     |
| 3         | 0.8                 | 82.1               | 97252.24                                   | 68751.6           | 29.31                    | 1.15     |

|    |      |      |          |         |       |      |
|----|------|------|----------|---------|-------|------|
| 4  | 0.7  | 82.6 | 89108.48 | 64363.2 | 27.77 | 1.15 |
| 5  | 0.6  | 83.2 | 86868.88 | 57049.2 | 34.33 | 1.15 |
| 6  | 0.55 | 83.6 | 74549.08 | 53392.2 | 28.38 | 1.15 |
| 7  | 0.5  | 84   | 69581.36 | 48272.4 | 30.62 | 1.15 |
| 8  | 0.45 | 84.4 | 65509.48 | 46078.2 | 29.66 | 1.15 |
| 9  | 0.38 | 85.2 | 56389.68 | 42421.2 | 24.77 | 1.15 |
| 10 | 0.3  | 85.7 | 48221.96 | 37301.4 | 22.65 | 1.15 |
| 11 | 0.2  | 86.0 | 40006.32 | 30718.8 | 23.22 | 1.15 |
| 12 | 0.1  | 86.3 | 22599.00 | 18285.0 | 19.09 | 1.15 |

Table 4 The semi-rigid models that optimised directly

| Model No. | Stiffness factor Fc | Strain energy (KJ) | Buckling load capacity (N/m <sup>2</sup> ) |                   | Imperfection sensitivity | Mass (t) |
|-----------|---------------------|--------------------|--|-------------------|--------------------------|----------|
|           |                     |                    | Without imperfection                       | With imperfection |                          |          |
| 13        | 1.0                 | 21.1               | 308274.1                                   | 170304.51         | 44.75                    | 1.34     |
| 14        | 0.9                 | 21.6               | 287196.2                                   | 165042            | 42.53                    | 1.33     |
| 15        | 0.8                 | 24.2               | 264245.3                                   | 145574            | 44.91                    | 1.288    |
| 16        | 0.7                 | 25.1               | 235065.6                                   | 134603            | 42.74                    | 1.277    |
| 17        | 0.6                 | 25.3               | 186774.1                                   | 113354.3          | 39.31                    | 1.275    |
| 18        | 0.55                | 25.1               | 190586.9                                   | 137659            | 27.77                    | 1.278    |
| 19        | 0.5                 | 27.4               | 170212.7                                   | 97804.08          | 42.54                    | 1.258    |
| 20        | 0.45                | 27.9               | 142241.4                                   | 115796.5          | 18.59                    | 1.254    |
| 21        | 0.38                | 28.9               | 139252.2                                   | 104946.4          | 24.64                    | 1.248    |
| 22        | 0.3                 | 35.3               | 102497.8                                   | 86441.94          | 15.66                    | 1.223    |
| 23        | 0.2                 | 42.1               | 78666.84                                   | 67955.33          | 13.62                    | 1.201    |
| 24        | 0.1                 | 60.0               | 36331.50                                   | 36490.50          | -0.44                    | 1.165    |

Table 5 The replaced models

| Model No. | Stiffness factor Fc | Strain energy (KJ) | Buckling load capacity (N/m <sup>2</sup> ) |                   | Imperfection sensitivity | Mass (t) |
|-----------|---------------------|--------------------|--|-------------------|--------------------------|----------|
|           |                     |                    | Without imperfection                       | With imperfection |                          |          |
| 25        | 1.0                 | 21.0               | 320192.1                                   | 173628            | 45.8                     | 1.337    |
| 26        | 0.9                 | 21.8               | 298186.2                                   | 168419.16         | 43.52                    | 1.337    |
| 27        | 0.8                 | 24.8               | 282180.48                                  | 173210.32         | 38.62                    | 1.337    |
| 28        | 0.7                 | 26.3               | 264168.96                                  | 142792.64         | 45.95                    | 1.337    |
| 29        | 0.6                 | 24.7               | 234149.76                                  | 155429.84         | 33.62                    | 1.337    |
| 30        | 0.55                | 24.6               | 219140.16                                  | 138748.44         | 36.69                    | 1.337    |
| 31        | 0.5                 | 27.1               | 198126.72                                  | 124594.48         | 37.11                    | 1.337    |
| 32        | 0.45                | 27.7               | 152120.96                                  | 109385.64         | 28.09                    | 1.337    |
| 33        | 0.38                | 28.6               | 144111.36                                  | 100704.24         | 30.12                    | 1.337    |
| 34        | 0.3                 | 35.0               | 123097.92                                  | 88550.28          | 28.07                    | 1.337    |
| 35        | 0.2                 | 41.8               | 96080.64                                   | 72923.76          | 24.10                    | 1.337    |
| 36        | 0.1                 | 58.7               | 55048.00                                   | 43407.00          | 21.15                    | 1.337    |

The data of each assembled lattice structures with semi-rigid joints are extracted after the optimisation, and compared with the initial structure and the optimised results. It should be noted that there are three different models here, the initial models with different joint stiffness, the semi-rigid models with different joint stiffness, and the replaced models with different joint stiffness. The initial models are the initial state of the structure, all the initial models have the same shape, however, the joint stiffness is different, which had been changed by changing the spring stiffness. The serial number of initial models are 1-12, as shown in Table 3. The semi-rigid models are the optimised results that take the assembled lattice structures as the optimisation object directly. All of the semi-rigid models have different shapes and different joint stiffness. The serial number of semi-rigid models is 13-24, as shown in Table 4. The replaced models are the optimised results that take a rigid lattice structures as the optimisation object. Then, the rigid joints of the structure are replaced by semi-rigid joints. All of the replaced models also have the same shape, but the different joint stiffness. The serial number of the replaced models are 25-36, as shown in Table 5. The significance of comparing the semi-rigid models and the replaced models is to explore which one is better during form finding of assembling lattice structures with semi-rigid joints – i.e., the result of optimising the assembled structure directly or the result that replacing the rigid joint with a semi-rigid joint after optimising the rigid structure.

In addition, to know the effect of initial geometric imperfection on the structural buckling load of the optimised structures, define the imperfection sensitivity as follows.

$$\varphi = \left| \frac{P_d - P_i}{P_i} \right| \times 100\% \quad (11)$$

Where  $P_d$  is the buckling load of the structure considering initial geometric imperfection;  $P_i$  is the buckling load of an intact structure without considering initial imperfection; the larger  $\varphi$  means the greater influence of initial geometric imperfection on the structural buckling load and the more sensitive the structure is. The imperfection is implemented according to the first-order eigenvalue buckling mode and the maximum value is 1/300 of the structural span.

It can be seen from the tables that as the optimisation proceeding, the total strain energy of each structure is decreasing, and decreasing rapidly in the initial stage of optimisation. Compared with the initial structure, the total strain energy of all the optimised structure is greatly reduced. Furthermore, the greater the joint stiffness is, the more the total strain energy of the structure will be reduced, which is reduced by up to 73.85% when the stiffness factor is 1.0.

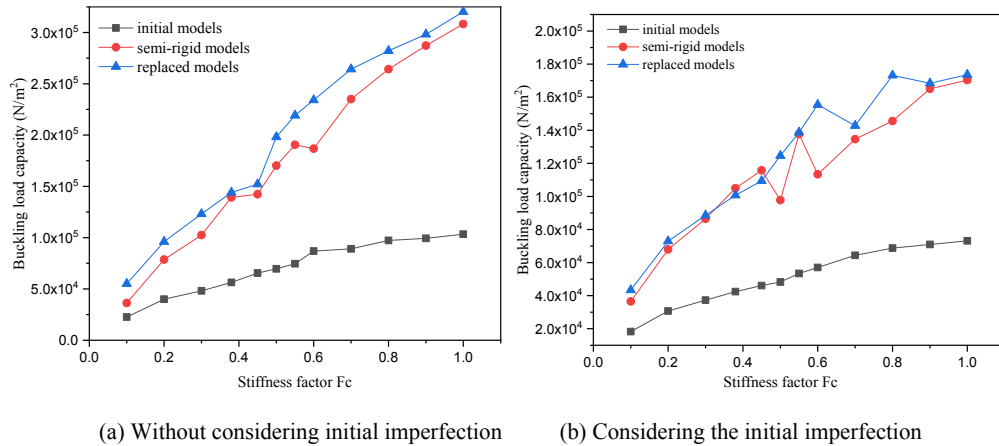


Fig. 8 Buckling load capacity of different models

For the mechanical properties of the optimised structures, the buckling load capacity of different models is shown in Fig. 8. Combined with the data in Tables 3-5, it is appreciated that under the same joint stiffness factor, whether the initial imperfection is applied or not, the buckling load capacity of the structure after form finding is greatly improved compared to the initial structure. If the initial imperfection is not considered, the buckling load capacity of the optimised structure has increased by up to 197.2% compared with the initial structure and thereafter the imperfection is applied, the buckling load capacity of the structure after

optimisation is increased by a minimum of 99.5% and a maximum of 132.6% compared with the initial structure. Furthermore, it is worth noting that, when the joint stiffness factor is equal to 0.45 and 0.38, and the imperfection is applied, the structural buckling load capacity of the semi-rigid model is 5% higher than that of the replaced model. Therefore, in this case, when the joint stiffness factor is equal to 0.45 or 0.38, the shape obtained by optimising the semi-rigid model directly is better than the result get by the replaced model. In addition, the figures also demonstrate that along with the increasing of the joint stiffness, the structural buckling load capacity is also increasing, which indicates that the joint stiffness has an important influence on the form finding of assembled lattice structures with semi-rigid joints. The larger the joint stiffness is, the easier it is to get the structure shape with higher buckling load capacity.

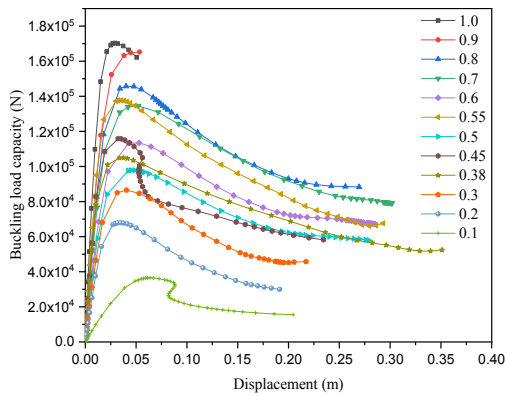


Fig. 9 Load-displacement curves of the semi-rigid models

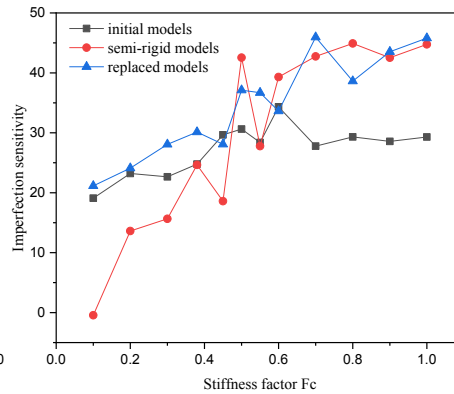


Fig. 10 Variation of imperfection sensitivity

The load-displacement curve of semi-rigid models is shown in Fig. 9, and depicts that structures with higher joint stiffness also have a higher buckling load capacity. Fig. 10 demonstrates the variation of imperfection sensitivity of different models. It can be seen that as the joint stiffness factor is increasing, the imperfection sensitivity of each model is gradually increasing. In particular, the initial models have the lowest imperfection sensitivity relatively, and the imperfection sensitivity of the replaced models is higher than that of the initial models. For semi-rigid models, when the stiffness factor is larger than 0.5, the semi-rigid model has a larger imperfection sensitivity than that of the initial model, in most cases. When the stiffness factor is smaller than 0.5, the imperfection sensitivity of the semi-rigid model is lower than that of the initial and the replaced model. This is the reason that when the stiffness factor equal to 0.38 or 0.45, the buckling load capacity of the semi-rigid model is slightly higher than that of replaced models.

### 4.3 Case 2

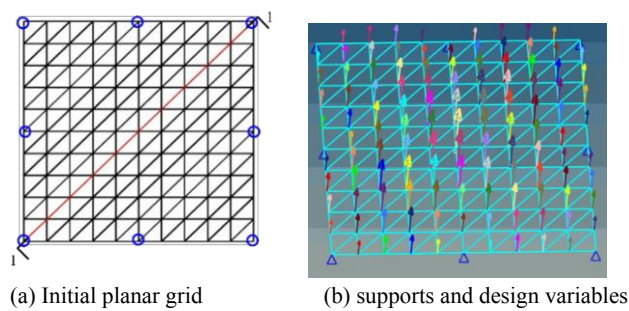


Fig. 11 Initial model

The assembled free-form single-layer lattice structure in last section, the structural initial shape has been roughly given. To verify the applicability of the proposed method for assembled lattice structure whose initial shape is not given, another assembled single-layer triangular lattice structure with plane quadrilateral is chosen as an example in this section. As shown in Fig. 11, the initial model is a quadrilateral with a length and width of 15m, and the four corners and the middle of the four edges are hinged, the load was distributed uniformly over the structure. The rod is a square steel tube with dimensions of 120mm×120mm×6mm made of steel grade Q345.

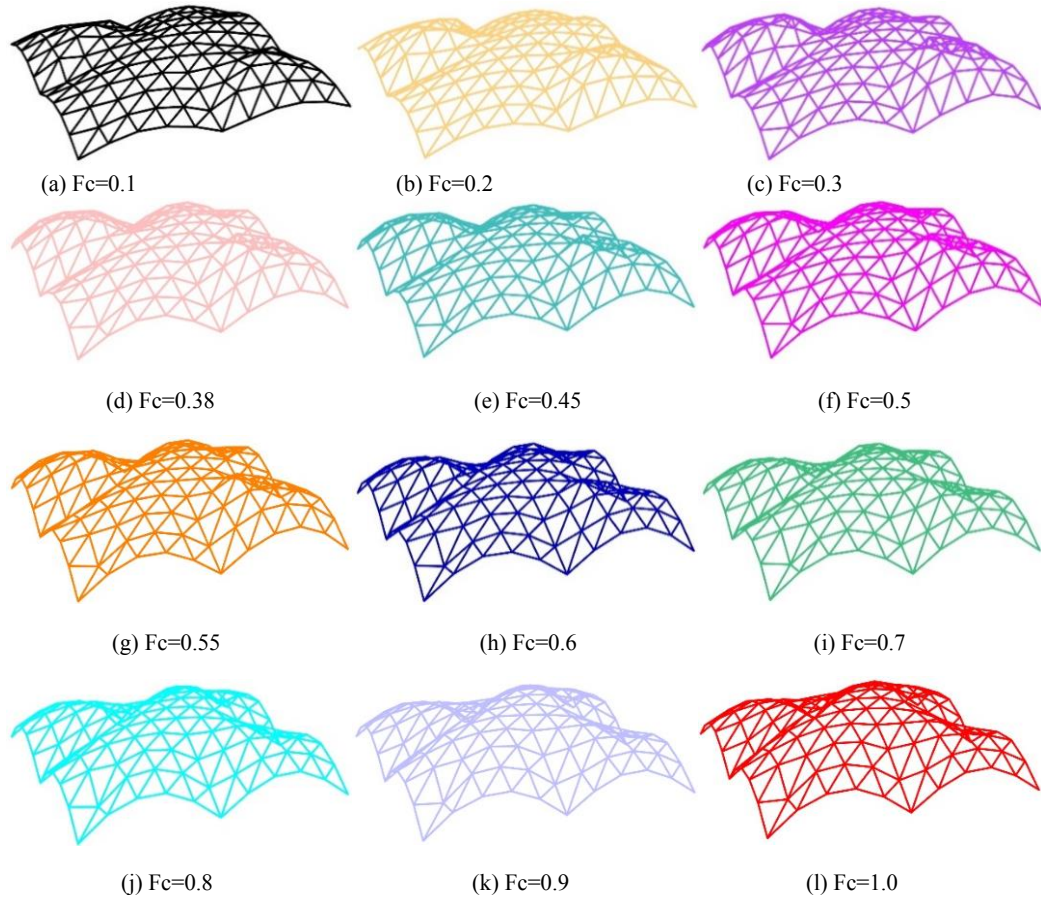


Fig. 12 Shapes obtained under the different stiffness factor

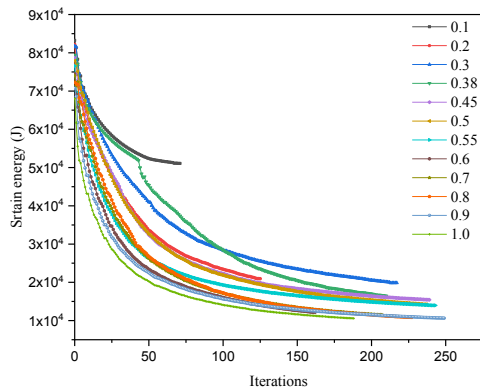


Fig. 13 Variation of strain energy

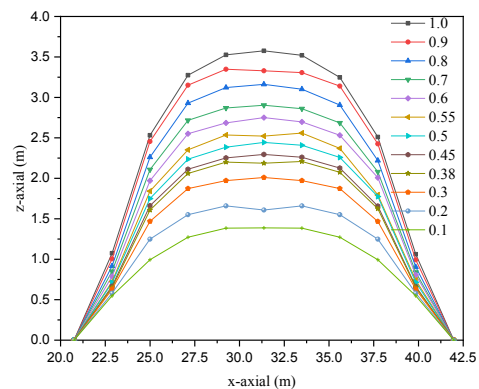


Fig. 14 Comparison of the structural cross-section

Taking the structural total strain energy as the object, the different joint stiffness is implemented by changing the virtual spring stiffness, and the stiffness factor is changed from 0.1 to 1.0. Finally, 12 optimal structural shapes under different joint stiffness are obtained, as shown in Fig. 12. It can be seen that after the optimisation, all structures with different joint stiffness have a certain degree of arching, and they have been transformed from planar quadrilateral to arched surfaces - that with four upwardly curved shapes. Moreover, as the joint stiffness increases, the amount of shape change of the structure after optimisation also increases, and then the degree of structural arching becomes higher. The variation of structural strain energy of different models is shown in Fig. 13, which shows that as the optimisation proceeds, the total strain energy of all structures is decreasing, and the greater the joint stiffness is, the more the total strain energy is reduced. When the stiffness factor is 1.0, the structural total strain energy decreases from 68045.8J to 10577.07J, with a decrease of 84.45%, and when the stiffness factor decreases to 0.1, the total strain energy of the structure decreases from 83236.4J to 51076.8J, only reduced by 38.6%. Fig. 14 depicts the comparison of the

structural cross-section; the cross-section line is shown in Fig. 11(a). The greater joint stiffness factor generates a higher structural height. When the joint stiffness factor equal to 1.0, the structure has the highest height of 3.57m.

Table 6 The semi-rigid models

| Model No. | Stiffness factor $F_c$ | Strain energy (KJ) | Buckling load capacity (N/m <sup>2</sup> ) |                   | Imperfection sensitivity | Mass (t) |
|-----------|------------------------|--------------------|--|-------------------|--------------------------|----------|
|           |                        |                    | Without imperfection                       | With imperfection |                          |          |
| 37        | 1.0                    | 10.57              | 56018.45                                   | 42165.33          | 24.7                     | 1.811    |
| 38        | 0.9                    | 10.63              | 45227.00                                   | 40640.60          | 10.14                    | 1.807    |
| 39        | 0.8                    | 10.80              | 42159.00                                   | 38309.70          | 9.13                     | 1.801    |
| 40        | 0.7                    | 11.52              | 38376.00                                   | 34924.50          | 8.99                     | 1.793    |
| 41        | 0.6                    | 12.18              | 34064.55                                   | 30379.05          | 10.82                    | 1.789    |
| 42        | 0.55                   | 13.96              | 29152.50                                   | 26110.50          | 10.43                    | 1.787    |
| 43        | 0.5                    | 14.22              | 24597.95                                   | 23075.10          | 6.19                     | 1.786    |
| 44        | 0.45                   | 15.45              | 25480.00                                   | 24440.23          | 4.08                     | 1.786    |
| 45        | 0.38                   | 16.44              | 26712.40                                   | 24596.00          | 7.92                     | 1.787    |
| 46        | 0.3                    | 19.85              | 23422.10                                   | 21689.20          | 7.40                     | 1.785    |
| 47        | 0.2                    | 20.94              | 14981.20                                   | 13936.00          | 6.98                     | 1.761    |
| 48        | 0.1                    | 51.07              | 8261.50                                    | 7675.21           | 7.10                     | 1.733    |

Table 7 The replaced models

| Model No. | Stiffness factor $F_c$ | Strain energy (KJ) | Buckling load capacity (N/m <sup>2</sup> ) |                   | Imperfection sensitivity | Mass (t) |
|-----------|------------------------|--------------------|--|-------------------|--------------------------|----------|
|           |                        |                    | Without imperfection                       | With imperfection |                          |          |
| 49        | 1.0                    | 10.57              | 57200.15                                   | 43355.24          | 24.20                    | 1.811    |
| 50        | 0.9                    | 10.61              | 54275.00                                   | 42487.90          | 21.72                    | 1.811    |
| 51        | 0.8                    | 10.69              | 51025.00                                   | 40753.70          | 20.13                    | 1.811    |
| 52        | 0.7                    | 11.34              | 48587.50                                   | 39019.50          | 19.69                    | 1.811    |
| 53        | 0.6                    | 11.13              | 44248.75                                   | 35117.55          | 20.64                    | 1.811    |
| 54        | 0.55                   | 12.79              | 39552.50                                   | 33816.90          | 14.5                     | 1.811    |
| 55        | 0.5                    | 13.34              | 35262.50                                   | 30782.05          | 12.71                    | 1.811    |
| 56        | 0.45                   | 14.56              | 32337.50                                   | 28180.75          | 12.85                    | 1.811    |
| 57        | 0.38                   | 15.35              | 27300.00                                   | 26013.00          | 4.71                     | 1.811    |
| 58        | 0.3                    | 18.34              | 26812.50                                   | 23845.25          | 11.07                    | 1.811    |
| 59        | 0.2                    | 19.97              | 22165.00                                   | 19943.30          | 10.02                    | 1.811    |
| 60        | 0.1                    | 43.45              | 13162.50                                   | 12355.85          | 6.13                     | 1.811    |

The data post-optimisation of the semi-rigid models and the replaced models are shown in Table 6 and Table 7, respectively. It is known through comparison that whether the semi-rigid model or the replaced model, their buckling load capacity increases with the increase of joint stiffness factor. However, independent of the joint stiffness, the buckling load capacity of the semi-rigid models is always lower than that of the replaced models, as shown in Fig. 15. In this case, a better structural shape with higher buckling load capacity is obtained by the replaced models. Fig. 16 shows the variation of structural imperfection sensitivity of different models. It suggests that the structural imperfection sensitivity becomes continuously higher as the

joint stiffness factor increases, and the imperfection sensitivity of semi-rigid models is always lower than that of the replaced models.

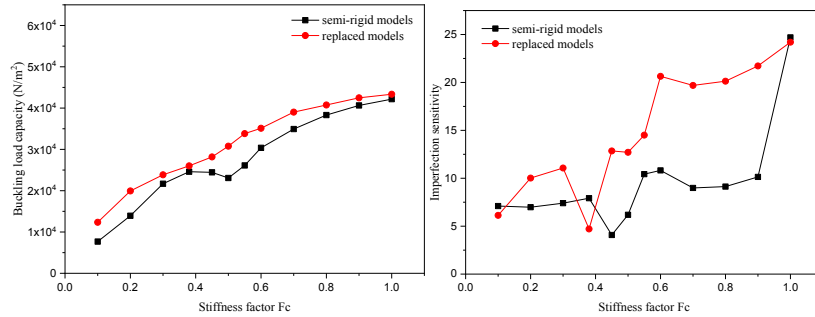


Fig. 15 Variation of buckling load capacity Fig. 16 Variation of imperfection sensitivity

## 5. Concluding remarks

In order to explore the influence of joint stiffness on form finding of assembled free-form single-layer lattice structures, a form finding method employing HyperWorks software was proposed in this paper. Initially, the actual joint stiffness was obtained through the prototype test. Then, the Beam-Virtual spring element was introduced and the FE model of the assembled free-form single-layer lattice structures was established. Then, the semi-rigid joint was simulated by virtual springs, and the effect of joint stiffness on the form finding was studied through changing the spring stiffness by a reasonable proportion. The main conclusions are as follows:

1. The joint stiffness will have a certain influence on form finding of assembled free-form single-layer lattice structures. Different joint stiffness will generate different structural shapes. Having greater joint stiffness, the structural shape variation will be larger, and a higher structural height will be obtained;
2. The greater the joint stiffness is, the higher structural buckling load capacity will be recorded post-optimisation, as well as it can result in the high structural imperfection sensitivity; and
3. In some cases, the buckling load capacity of the semi-rigid model is higher than that of the replaced model, but the increase is limited - only about 5%. In general, the buckling load capacity of the semi-rigid model is lower than that of the replaced model. On the other hand, the structural imperfection sensitivity of the replaced model is higher than that of the semi-rigid model.

This study creates the potential to consider the real semi-rigid behaviour of connections during form finding and exploit the benefits, resulting in more accurate and fully optimised shapes of reticulated structures.

## Acknowledgments

This research was financially supported by the Natural Science Foundation of China under grant numbers 51978151, by the Colleges and Universities in Jiangsu Province Plans to Graduate Research and Innovation KYLX16\_0254, by the Fundamental Research Funds for the Central Universities, and by a Project Funded by the Priority Academic Program Development of the Jiangsu Higher Education Institutions.

## References

- [1] Rippmann, M. Funicular Shell Design: Geometric approaches to form finding and fabrication of discrete funicular structures. ETH Zurich. 2016.
- [2] Lopez, E.A. and Troup, K. Aluminum lattice structures: Developments and innovations ion clear span roof solutions. International Symposium on Conceptual Design of Structures. 1996.
- [3] S. Stephan, J.Sánchez-Alvarez, K. Knebe. Reticulated structures on free-form surfaces. <http://www.mero.de>. 2004.
- [4] Abdelwahab, M. and Tsavdaridis K.D. Optimised 3D-Printed Metallic Node-Connections for Reticulated Structures. The 9th International Conference on Steel and Aluminium Structures. 2019, 3-5 July 2019, Bradford, UK (10.31224/osf.io/jkexd)

- [5] Seifi, H. Topology optimisation and additive manufacturing of structural nodes of lattice structures. 2019.
- [6] See, T. Large displacement elastic buckling of space structures. Doctoral Thesis, University of Cambridge. 1983.
- [7] El-Sheikh, A.I. Numerical analysis of space trusses with flexible member-end joints. *International Journal of Space Structures*. 1993, 189-197.
- [8] Loureiro, A., Goni, R. and Bayo, E. A one-step method for buckling analysis of single layer lattice structure with semi-rigid connections. *Proceedings of the fifth international conference of space structures*, London, 2002, 1481.
- [9] L'opez, A., Puente, I. and Serna Miguel, A. Direct evaluation of the buckling loads of semi-rigidly jointed single-layer latticed domes under symmetric loading. *Engineering Structures*, 2007, 29(1), 101–109.
- [10] L'opez, A., Puente, I. and Serna Miguel, A. Numerical model and experimental tests on single-layer latticed domes with semi-rigid joints. *Computers and Structures*, 2007, 85(7–8), 360–374.
- [11] Kato, S., Mutoh, I. and Shomura, M. Collapse of semi-rigidly jointed reticulated domes with initial geometric imperfections. *Journal of Constructional Steel Research*, 1998, 48(2-3):145-168.
- [12] Lightfoot, E. and LeMessurier A.P. Instability of Space Frames Having Elastically Connected and Offset Members. *Proceedings of International Conference of Space Structures*, University of Surrey, UK. 1975, 143-149.
- [13] Guo, X., Xiong, Z. and Luo Y. The design method and detailed requirements of bearing capacity of aluminum alloy gusset joint. *Journal of Tongji University*. 2015, 43. 47-53.
- [14] Guo, X., Xiong, Z. and Luo, Y. Experimental investigation on the semi-rigid behavior of aluminium alloy gusset joints. *Thin-Walled Structures*, 2015, 87:30-40.
- [15] Ma, H., Fan, F., Chen, G., Cao, Z., and Shen, S. Numerical analyses of semi-rigid joints subjected to bending with and without axial force. *Journal of Constructional Steel Research*, 2013, 90(5), 13–28.
- [16] Feng, R., Ye, J. and Zhu, B. Behavior of bolted joints of cable-braced lattice structures. *Journal of Structural Engineering*. 2015, 141(12): 04015071.
- [17] Feng, R., Liu F, Yan G, et al. Mechanical behavior of Ring-sleeve joints of single-layer reticulated shells. *Journal of Constructional Steel Research*, 2017, 128: 601-610.
- [18] Feng, R., Ge J. and Ye, J. Shape optimization of free form cable-braced lattice structures. *China Civil Engineering Journal*, 2013, 46 (4): 64-70.
- [19] Feng, R., Ge, J., Hu, L. and Ye, J. Multi-objective shape optimization of free-form cable-braced lattice structures with B-spline method. *China Civil Engineering Journal*, 2015, 48(6):1-8.
- [20] Hawdon-Earl, S. and Tsavdaridis, K.D. Form Finding and Dimensioning of Reinforced Concrete Shell Roof for Akrotiri (Santorini). *Journal of the International Association for Shell and Spatial Structures (IASS)*. 2018, 59(4), 198.
- [21] Wang, X., Feng, R., Yan, G., Liu, F.C. and Xu, W.J. Effect of joint stiffness on the stability of cable-braced lattice structures. *International Journal of Steel Structures*, 2016, 16(4): 1123-1133.